LAWRENCE
LIVERMORE
NATIONAL
LABORATORY

UCRL-BOOK-223307

Chapter 9: Model Systems for Formation and Dissolution of Calcium Phosphate Minerals

C. A. Orme, J. L. Giocondi

August 2, 2006

Handbook of Biomineralization

Updated October 14, 2003

Chapter 9: Model Systems for Formation and Dissolution of Calcium Phosphate Minerals

Christine A. Orme and Jennifer L. Giocondi
Lawrence Livermore National Laboratory
7000 East Ave.
Livermore, CA 94550
51,000 characters. 5 Tables, 9 figures
p=(51,000+18000+5000)/2800 = 26 pages.

Key words: Calcium phosphates, scanning probe microscopy, solution speciation, kinetics, crystal growth, nucleation, impurities, brushite

9.1 Abstract

Calcium phosphates are the mineral component of bones and teeth. As such there is great interest in understanding the physical mechanisms that underlie their growth, dissolution, and phase stability. Control is often achieved at the cellular level by the manipulation of solution states and the use of crystal growth modulators such as peptides or other organic molecules. This chapter begins with a discussion of solution speciation in body fluids and relates this to important crystal growth parameters such as the supersaturation, pH, ionic strength and the ratio of calcium to phosphate activities. We then discuss the use of scanning probe microscopy as a tool to measure surface kinetics of mineral surfaces evolving in simplified solutions. The two primary themes that we will touch on are the use of microenvironments that temporally evolve the solution state to control growth and dissolution; and the use of various growth modifiers that interact with the solution species or with mineral surfaces to shift growth away from the lowest energy facetted forms. The study of synthetic minerals in simplified solution lays the foundation for understand mineralization process in more complex environments found in the body.

9.2 Introduction

Organisms use complex, biologically regulated processes with many feedback loops to create microenvironments that induce *nucleation* and *growth*. This is often achieved at the cellular level by generating organic templates and solution states that in turn control crystallization. Similarly *dissolution* processes, such as found in healthy bone remodeling, or as found in diseases such as caries and osteoporosis, reflect an underlying chemistry that has been biologically manipulated to favor resorption. In general, solutions, proteins, and templates act together to control growth and dissolution. In this chapter we focus on the role of the solution as a model environment for modifying growth kinetics and thermodynamics of calcium phosphate minerals.

Model solutions represent aspects of body fluids such as serum, urine, or saliva, but do not contain the full complement of ions and proteins found in biological systems. There are many virtues of model solutions, chief among them reproducibility and the ability to explore systematic variations about a norm. The use of simplified environments is not meant to mimic biosystems so much as to address how plausible changes in the solution

chemistry impact mineralization This simplification has the advantage of allowing one to ask specific questions such as: *How does citrate impact brushite crystallization?* – A query that complements biological or medical motivated questions such as: *Does citrate act as a therapeutic for kidney stone formation*? The study of synthetic minerals in simplified solution lays the foundation for understand mineralization process in more complex environments found in the body.

This chapter begins with a discussion of solution speciation in body fluids and relates this to important crystal growth parameters such as the supersaturation, pH, ionic strength and the ratio of calcium to phosphate activities. We then discuss how scanning probe microscopy can be used to investigate surface kinetics of mineral substrates evolving in simplified solutions. The goal of this style of experiment is to develop an understanding of the mechanisms by which growth modifiers alter crystal growth.

9.3 Calcium phosphate phases found in biology

Organisms have adopted various strategies for creating hard tissues suitable for bearing loads. Marine organisms such as mollusks and algae have adapted to take advantage of materials in their external environment by creating exoskeletons and grinding appendages composed of calcium carbonates or silica. For example the layered nacre of the abalone shell is composed of alternating sheets of crystalline calcite and aragonite intertwined with organic binders; the intricate frustule of the diatom is a glass composed of very pure silica; and the grinding teeth of the sea urchin are composed of calcite but hardened with "impurities" of magnesium[1]. These examples serve as archetypes of the complex structures found in nature due to the bioavailability of carbonates and silicates in oceans (and lakes). By contrast, the *interiors* of organisms are bathed in phosphate, part of our adenosine triphosphate (ATP) driven energy cycle. As a result, our body fluids are consistently supersaturated with respect to calcium phosphates and our endoskeletons and other load bearing mineralized tissue like teeth have evolved to reflect this chemistry.

Whether carbonate, silicate, or phosphate, biominerals adopt interesting strategies to expand the versatility of the relatively simple base materials. In the examples above, the abalone shell gains strength and limits crack propagation because it is an organic-inorganic composite composed of two polymorphs; the diatom makes use of amorphous instead of crystalline materials; and the sea urchin uses impurities to confer changes in mechanical properties. These strategies can also be found paralleled in calcium phosphate structures. For example, bones tune elasticity and hardness with a collagen-mineral composite[2]; matrix vesicles, which mineralize bone, are thought to store stabilized amorphous calcium phosphate[3]; and teeth are less soluble when small concentrations of fluorine incorporate into their outer layers[4]. There have been several books and reviews beyond the current volume that discuss the general assembly strategies that lead to complex biomaterials[5-8] and it is not our purpose to review them here. The two primary themes that we will touch on are the use of microenvironments that temporally evolve the solution state to control growth and dissolution; and the use of various growth modifiers that interact with the solution species or with mineral surfaces to shift growth away from the lowest energy facetted forms that are defined by the crystal Wulff plots.

The calcium phosphate phases of interest in biology include amorphous calcium phosphate, as well as several crystalline forms with names, abbreviations and some physical properties summarized in Table 9.1. These materials have been thoroughly reviewed by several authors[9, 10]. Typically, biogenic calcium phosphate is not pure, but rather substituted, as shown for the apatites: bone, enamel, and dentine.

For the most part healthy mineralized tissues are hierarchical composites composed principally of magnesium and carbonate substituted hydroxyapatite closely associated with a collagen matrix. Dentin and cementum in the tooth, and the various forms of bone[12] are all approximately 70 wt.% apatite with 20% collagenous matrix and 10% water. Enamel, which unlike the other tissues, contains no cells or pores is almost 95 wt. % mineral[9]. Enamel also differs in that it is associated with proteins enamelin and ameliogenin rather than collagen. While these biomaterials have broad similarities, they differ in important details including their minor elements, water composition, and degree of crystallinity[9].

Table 9.1 provides solubility products for synthetic and biogenic calcium phosphate phases. As noted in the table, the biogenic apatite, enamel, dentine, and bone, are impure and non-stoichiometric. Major impurities (in weight percent) include carbonate (3.5-7.4%), which has been shown to substitute for phosphate, as well as sodium (0.5-1%), magnesium (0.4-1.2%), potassium (0.03-0.08%), chloride (0.01-0.3%) and fluoride (0.01-0.06%)[13, 14]. The impurities typically shift the solubility making biogenic apatite considerably more soluble than synthetic HAP. Despite the impurities, one needs only to look at a skeleton to know that bones and teeth are sparingly soluble. And yet, although skeletons can last thousands of years in the environment, within the body, bones are constantly being dissolved from one location and deposited in another as a response to mechanical stress and hormonal environment. On average, bones are dissolved and rebuilt every 30 years (based on 3% per year rate for cortical bone in healthy adults). To accomplish this, the body uses specialized cells and vesicles, to create microenvironments that regulate Ca^{2+}, HPO_4^{2-}, and H^+ to favor crystal growth or dissolution.

Apatite is the dominant calcium phosphate phase found in mineralized tissue; however, other transitory phases are postulated in healthy mineralization and are found stabilized for longer duration in pathological mineralization. A few examples, by no means exhaustive, are indicated in Table 9.2. Model solutions that may serve as a starting point for investigating the mineralization dynamics are also indicated.

9.4 Solution chemistry in the body

9.4.1 Solution speciation

Solution speciation is the starting point for quantitative solution crystal growth. To model the thermodynamic properties of a solution it is first necessary to know the solubility product (K_{sp}) and the association constants (K_a) for all possible solid and solution species. Due to the many solid calcium phosphate phases (Table 9.1) and solution complexes (not

shown), calcium phosphate chemistry is extremely complicated even in simplified, model environments. And despite the maturity of this field the databases continue to evolve as new methods improve the accuracy of solubility measurements [20].

Solution speciation techniques, which have been made routine with commercial and shareware programs, calculate the concentrations and activities of all solution ions and complexes from a list of initial reactants and a database of potential reactions with their respective association constants and solubility constants[26]. Typically a solution is described in terms of ion or salt concentrations (such as in Table 9.3) however it is the activities that determine the full speciation. Speciation shown in this chapter uses GeoChemists' WorkBench[27] with an extended Debye-Huckle formulae[28] to define the activity coefficients.

9.4.2 Crystal growth parameters

Once speciation has been accomplished, the activities can be recast in terms of parameters that affect crystallization (lower half of Table 9.3). In general these parameters can affect both the solution speciation (which is a thermodynamic consideration) as well as the surface of the mineral (which can be either a thermodynamic consideration such as shifting the hydrated state of the surface with pH, or a kinetic consideration affecting the activation barriers associated with incorporation). This section will briefly discuss the roles of supersaturation, pH, ionic strength and ratio of cations to anions. The effects of each of these parameters are summarized in Table 9.4. The effects of additives will be covered in section 9.6.

The most important crystallization parameter is the thermodynamic driving force or the *supersaturation*. The supersaturation, $\sigma = \Delta\mu / kT$, is a unitless number proportional to the chemical potential difference associated with molecules transferring from the bulk solution to the bulk solid phase and can be determined from speciation calculations. Three related representations for the driving force are found in the literature: the *supersaturation*, the *supersaturation ratio*, and the *relative supersaturation.* It is instructive to spend a moment to define the relationship between these terms.

The supersaturation ratio can be computed from the solution speciation results by disallowing precipitation so that all ions remain in the solution phase. From this one can calculate the ion activity products (IP) for minerals of interest. The *supersaturation ratio*, S is then given by

$$S = \frac{IP}{K_{sp}}, \quad S_{HAP} = \frac{\{Ca^{2+}\}^5\{HPO_4^{2-}\}^3\{OH^-\}^1}{K_{sp,HAP}}, \quad S_{DCPD} = \frac{\{Ca^{2+}\}\{HPO_4^{2-}\}}{K_{sp,DCPD}}, \qquad (9.1)$$

where the supersaturation ratio for hydroxyapatite (half unit cell) and brushite are shown explicitly. For S=1, the mineral and solution are in equilibrium, for S<1 the solution is undersaturated and the mineral will dissolve, and for S>1 the solution is supersaturated and the mineral will grow. Usually the half unit cell notation is used for octacalcium phosphate and the various apatites. In this representation $K_{sp,HAP} = 10^{-58.65}$ (as shown in Table 9.1) and 9 growth units are denoted in the activity product. In the full unit cell representation 18 growth units appear in the activity product and the solubility product is correspondingly squared, $K_{sp,HAP,full} = 10^{-117.3}$. From this example one can see that

$S_{HAP,full} = S_{HAP,half}^2$, which highlights the necessity of normalizing by the number of growth units (n) when making comparisons between minerals with different numbers of growth units. Traditionally the supersaturation is written per molecule rather than per growth unit and is related to S through $\sigma = \Delta\mu / kT = \ln S$. To allow comparisons between phosphate phases, it is useful to define a driving force that is normalized for the number of growth units in the unit cell (n),

$$\sigma_{gu=} \frac{\Delta\mu_{gu}}{kT} = \ln S^{\frac{1}{n}} \tag{9.2}$$

where 'gu' denotes growth unit. Notice that for S~1 (i.e. near saturation) the logarithm can be expanded (lnx~1-x for x~1) leading to what is commonly termed, the relative supersaturation, defined as:

$$\sigma_{rel} = S^{1/n} - 1, \tag{9.3}$$

In this chapter we will use equation 9.2 because of the broad range of supersaturation ratios found in body fluids.

In equilibrium $\sigma_{gu}=\sigma_{rel}=0$ however most solutions have a metastable region region, where the $\sigma>0$ and yet the supersaturation is not high enough for crystals to spontaneously precipitate from solution phase. Above a supersaturation threshold the These regimes are schematically represented in Figure 9.1 plotted against the calcium to phosphate activity ratio to highlight the fact that a solution with a fixed supersaturation can be either phosphate rich (left side of the graph) or calcium rich (right side of the graph). Thermodynamically these solutions will have the same driving force for growth but the kinetics can differ substantially.

The second parameter, *pH* affects both the solution as well as the mineral surface. In the solution, a shift to lower pH will lower the saturation state by shifting the balance of phosphate species from PO_4^{3-} to HPO_4^{2-} to $H_2PO_4^-$. At the mineral surface the pH can shift the surface charge by changing the distribution of proton and hydroxyl groups hydrating the interface. For hydroxyapatite the point of zero charge (in solutions without calcium) occurs at pH=7.3. For more alkaline solutions the surface is negatively charged whereas for more acidic, it is positively charged. However, ions other than H^+ and OH^- can adjust surface charge and in calcium containing solutions, the Ca^{2+} ions bind to the surface for pH >7, leaving the surface neutral rather than negative (provided calcium remains in solution)[29].

The third parameter, *ionic strength* plays a role in screening both ion-ion electrostatic interactions in solution (which is accounted for by the activity coefficient) and electrostatic interactions between ions in solution and the surface. The ionic strength of a solution, I, is defined as

$$I = 1/2 \sum_i [i] z_i^2,$$

where [i] is the concentration and the z_i the charge, of each ionic species, i. The Debye length sets the screening range at the mineral surface and thus sets a length scale for the electric field generated at the charged surface. In most biological systems the ionic strength is near 0.15M corresponding to a Debye length of approximately 1nm.

Temperature is generally an important crystal growth parameter although it is not a variable in a regulated environment such as the body. Many solubility products and association constant are temperature dependent thus so is the solution speciation. Temperature also effects the kinetics of adsorption, desorption, and diffusion. Within transition state theory, these motions are typically modeled as activated hopping processes where the probability of making the jump can be written as $P = \nu(T)e^{-E_a/kT}$. The attempt frequency, υ, is weakly temperature dependent and is typically treated as independent of temperature. Thus, the primary temperature dependence is the exponent. However, in biological systems temperature is regulated and remains nearly constant (37ºC for humans) thus while temperature can be used as a tool in vitro to measure activation barriers (E_a), it is not a control used *in vivo*.

Parameters such as the *ratio* of calcium and phosphate activities acknowledge that growth rates may not be dictated simply by the supersaturation and the surface energies but rather that kinetics may play a role. In principle ion ratios can affect growth rates, growth shape, and the transformation of meta-stable phases. The growth of a multi-species crystal relies on the relative rates of adsorption and desorption of the various ions or growth units that make up the unit cell. For a simple salt such as NaCl the growth units are the Na^+ and Cl^- ions. However in general the growth units represent the pathway with the lowest activation barrier that allows an ion to move from the solution state to the solid state and vice-versa. In a binary ionic compound such as brushite, it is tempting to think of the growth units as Ca^{2+} and HPO_4^{2-}, but it is possible that in the process of shedding waters of hydration and incorporating into the solid that the activation barrier is lower for a multi-step process wherein one of the other phosphate complexes adsorbs and then adds or sheds a hydrogen. The graphs shown in this chapter use the ratio of the calcium ion activity to the total phosphate ion activity ($\{P_i\}=\{H_2PO_4^-\} + \{HPO_4^{2-}\} + \{PO_4^{3-}\}$) to accommodate the uncertainty in rate-limiting ions. Many groups have shown that ion ratios play a role in kinetics and some progress has been made at modeling these effects[30]; however, most crystal growth models assume a single species and more work is needed to fully describe multi-component crystals.

9.4.3 The speciation of body fluids

The compositions and resultant crystal growth parameters for common body fluids including serum, saliva, enamel fluid, plaque, and urine are summarized in Table 9.3. Note that the calcium, phosphate and pH values have broad ranges reflecting temporal and population variability. Saliva, plaque fluid and urine are especially affected by external factors such as diet and this is reflected in their wide range of values. The exceptions are the pH of serum, which is regulated, and enamel fluids where little information is available. Table 9.3 also lists the range of values of the important crystal growth parameters as are determined by speciating the average solution chemistries over all combinations of maximum and minimum calcium and phosphate concentrations and pH.

One way of summarizing the variability of parameters in these solutions is to construct a map. The solutions maps in Figure 9.2 express the supersaturation (per growth unit) as a

function of the calcium to phosphate activity and the pH for HAP (low solubility) and DCPD (high solubility). These are shown for the body fluids listed in Table 9.3. The bounding areas of Figure 9.2a were determined by speciating all combinations of the maximum and minimum calcium and phosphate concentrations and pH values in the presence of the average concentrations of the other ions listed. The curves in Figure 9.2b were generated by speciating the average concentrations of all listed ions over the entire normal pH range. Note that HAP and DCPD were chosen to display as bounding cases and that the minerals with intermediate solubilities will fall between these plotted range of values.

From these maps we can make several observations. First, most body fluids are richer in phosphate than calcium with serum being the exception. In serum the Ca/PO_4 ratio is near that found in bone (1.66) and likely plays a role in creating crystals with this stoichiometry during the body's cycle of bone reformation. Secondly, HAP is supersaturated in all fluids over almost their entire range, with the result that under most conditions our bones and teeth are stable. And in fact, solution conditions need to be explicitly modified to dissolve biological apatites as will been seen in the example of the osteoclast. DCPD, on the other hand, lies nearer to the saturation border and is both under- and super-saturated. In healthy conditions, as represented by these solutions, HAP is always more supersaturated than DCPD; however at lower pH values one can see that the HAP and DCPD stability lines will cross due to the shifts in relative concentrations of PO_4^{3-} and HPO_4^{2-}. It is thus possible under pathological conditions for DCPD to be more stable than HAP, although this requires both higher acidity and higher calcium and phosphate concentrations than is normal. Table 9.2 suggests some instances where DCPD forms; however it is not clear whether these are cases where DCPD is thermodynamically stable or a transitory phase.

Another interesting point is that crystals do not normally nucleate in fluids such as serum despite the fact that they are highly supersaturated; this can be attributed in part to the metastable region where the probability of homogeneous nucleation is small, and in part to the presence of nucleation inhibitors (such as proteins) that are not accounted for in a thermodynamic map. In some ways the solution maps of normal, easily accessible body fluids give the regions over which nothing much happens – apatites neither dissolve, nor do they nucleate. One of the more difficult aspects of biomineralization is determining the composition and time-evolution of specialized local environments where crystals are forming or resorbing. Several possible pathways have been postulated that illustrate how the solution conditions might be manipulated to favor nucleation and dissolution; some of these are shown in Table 9.5. The remainder of this section will describe, as an example, the possible mechanisms at play when bone minerals are formed and resorbed.

It is currently thought that the growth of individual crystals for bone mineralization takes place in two stages - nucleation and subsequent growth- and that these processes occur in different solution environments[31, 32]. The nucleation phase occurs in the regulated environment of small (~100nm), fluid-filled, phospholipid "containers" called matrix vesicles (MV) that are released by osteoblast cells into the surrounding tissue termed the osteoid. In general, more favorable nucleation environments can be created by increasing

calcium or phosphate concentrations, creating suitable templates that reduce interfacial energy, or reducing inhibitor concentrations; within the interior of the MVs one (or several) of processes must occur. Amongst several potential pathways for initiating nucleation[32-34], two of them involve the enzyme alkaline phosphatase. Alkaline phosphatase (ALP) is produced by osteoblasts and can react with phosphorylated proteins to produce free phosphate. In principle this would be a mechanism that could be used to regulate phosphate concentration[35]. On the schematic solution map (Figure 9.1), the initiation of nucleation implies increasing the supersaturation above the metastable line into the labile region. Alternatively, or in parallel, ALP hydrolyzes pyrophosphates, which are known mineralization inhibitors thus lowering the barrier to nucleation. Inside the MV, the first phase to form is amorphous calcium phosphate, which then transforms into apatite with a needle-like morphology. At some point the MV membrane is disrupted and the apatite needles finish their growth in the surrounding serum-like solution. This example highlights one route for separating nucleation from growth when the two processes have different solution requirements.

Controlled dissolution also occurs in an occluded environment as seen under an osteoclast cell during mineral resorption. Osteoclasts actively dissolve bone through a complex set of linked processes that ultimately produce high concentrations of HCl in an occluded region abutting the bone. To generate these high local concentrations of acid, the cell seals off a region known as the resorption lacuna and uses a vacuolar-like proton pump (H^+-ATPase) to transport H^+ against a gradient. Chloride channels maintain charge balance[36-38]. Within the resorption lacuna, the pH drops to 4.5[39]. Figure 9.3 depicts the change in saturation state associated with reducing the pH of a serum-like solution. The band spans a range of solubilities from the least soluble synthetic FAP to the most soluble dentine; the actual solubility will depend upon the bone composition. A more full simulation of this process would also need to account for other changes in the solution such as contributions from the dissolving mineral. However from this simple titration one can see that that the solution moves from being supersaturated with respect to apatite to being undersaturated, thus favoring dissolution. Similar pH-mediation is found in caries where bacterial colonies on the teeth produce lactic and acetic acid as part of their metabolic cycle.

9.4.4 Limitations of speciation modeling

There are a number of limitations to keep in mind particularly with respect to modeling mineralization within the body. First, this is a thermodynamic approach and if reactions are slow the solution may not reflect its thermodynamic values. Similarly, mineralization inhibitors typically slow kinetics and are not accounted for in a thermodynamic model. Also, inherent to any speciation modeling, the calculations reflect the quality and completeness of the databases that contain the solubility products and the association constants. Speciation becomes more difficult as one includes proteins and organic surfaces because the association constants are rarely known for these materials. Similarly, we have imperfect knowledge of the *local* solution environments where mineralization occurs. Typical compositions and ranges of bodily fluids such as blood serum and urine are accessible and well documented, however the time evolution of the solution

composition in an occluded environment such as within a matrix vesicle or underneath an osteoclast is less well known. Nevertheless, quantitative crystal growth relies on speciation and a great number of biomineralization studies could be more easily compared and made more rigorous by its application.

9.5 Measuring Crystal growth

There are a limited number of *in situ* techniques that are viable in a fluid environment and that quantify crystallization dynamics. These include optical spectroscopies such as Raman and Fourier-transform infrared spectroscopy; diffraction techniques, such as x-ray or neutron (although these typically require a dedicated facility), interferometry, and imaging techniques such as video microscopy and scanning probe or atomic force microscopy (SPM, AFM). In addition a number of solution probes have been developed to monitor aspects of solution chemistry, such as pH probes and ion selective electrodes. Most kinetic measurements have been obtained on bulk powders that reflect a distribution of facets and surface morphologies.

Bulk crystallization experiments can either be classified either as *free drift* where the solution composition varies due to nucleation and growth, or *constant composition* (CC)[40, 41] where changes in the solution composition are monitored and compensated as the crystallization process occurs. In a seeded CC experiment, crystals (with known surface area) are placed in a temperature controlled growth chamber with an automated titration system to maintain a constant pH or other ion selective electrode reading. As the crystals grow, consuming calcium and phosphate from solution, the pH (or $\{Ca^{2+}\}$) shifts. Based on these changes (and knowledge of the seed materials), calcium and phosphate ions are automatically added to the solution to balance the material grown. The crystal growth rate is obtained from the additions after normalizing by the crystal surface area; noting that the crystal surface area changes throughout the experiment and thus must be calculated or measured. Variations on the seeded CC method allow the measurement of dissolution rates, nucleation rates, and growth rates for multiple species.

Constant composition experiments have clear advantages for quantitative crystal growth. They allow growth rates to be measured systematically as a function of the parameters delineated in Section 9.4.2; they test and develop the speciation database; and they determine which additives act as inhibitors. Although CC has arguably done more than any other single method to develop the quantitative physical chemistry of calcium phosphates, it is a bulk method with a limited ability to deduce how and where molecular changes occur. The SPM has emerged as a complementary technique that, like CC, quantifies kinetics in a fluid environment but measures the crystal surface rather than the solution state.

Scanning probe microscopy measures surface morphology by rastering a cantilever over the surface and detecting its deflection. The lateral resolution is limited by the probe used to scan the surface and is typically 10nm; thus the individual growth units (such as Ca^{2+}, HPO_4^{2-} or PO_4^{3-}) of a growing crystal are not resolvable except when the crystal is composed of large building blocks such as proteins[42]. What makes the SPM valuable

for crystal growth is its sub-angstrom z-resolution, making it capable of measuring atomic steps. For *in situ* work, temperature and pH-controlled solutions are pumped through a fluid cell (Figure 9.4) while the crystal is being imaged. The flow rate is adjusted until the surface dynamics are independent of flow ensuring that the system is not mass-transport limited. This also ensures that the crystal is responding to a solution with the same (constant) composition as the reservoir. Figure 9.5 shows a typical AFM image of atomic steps emanating from a dislocation source. In this case the surface is the [010] face of a DCPD crystal and the 0.38 nm steps are readily imaged even when scanning relatively fast (~12 seconds per image). Sequential images make a movie that captures the trajectory of the growing crystal steps allowing direct measurement of the step velocities in the different crystallographic directions. Similarly, when the solution is undersaturated, etch pits form (Figure 9.6) and their dissolution can be monitored. Both growth hillocks and etch pits reflect the underlying symmetry of the crystal (Figure 9.5c) which, for the case of DCPD has three steps forming a triangle.

The ability to monitor step dynamics also enables several other fundamental measurements beyond step velocity and morphology. The reader is referred to several reviews[43, 44] and books[45] that cover these topics. In brief, one important parameter that can be measured is the length needed for a step to propagate. When the step is in equilibrium this length is termed the *critical length* and reflects a balance between the reduction of energy associated with the chemical potential difference between solution and solid, and the increase in energy associated with creating a step-edge. In this case, $L_c \propto \gamma / \Delta\mu$ where γ is the step-edge free energy; from this relation, the step free energy can be obtained by measuring the critical length as a function of supersaturation[46]. If the step is not in equilibrium, but rather has a low probability of moving due to kinetics, then the step length is instead related to the probability of nucleating a kink[47]. There is growing evidence that this is a common case for sparingly soluble materials such as calcium phosphates[48]. However, the theoretical description of this case is still under development.

In the next section we will discuss how SPM can be used to augment bulk rate measurements by helping to pinpoint the mechanisms by which impurities or additives interaction with the growing crystal surface.

9.6 Impurity Interactions

Thus far we have discussed the speciation and growth parameters associated with base solutions without inhibitors or growth modifiers such as proteins. Calcium phosphates growth and stability is influenced by a great many inorganic and organic species. Some of the major modifiers are a) the ions that are found incorporated into biogenic apatites (such as Mg, Cl, Na, CO_3, K, F), b) proteins (such as collagen, ameliogenin, albumin), c) molecules with phosphate moieties (such as pyrophosphate), and d) molecules with carboxyl moieties (such as carbonate, citrate).

There are several generic ways in which an adsorbate can affect growth: it can substitute for similar ions within the crystal which may induce strain[49]; it can bind to the surface hindering or pinning step motion; and it can adsorb to steps such that the composite has

new equilibrium facet directions (i.e. by acting like a surfactant)[50]. In addition, some adsorbates may act as local ion sources, thereby effectively increasing the local supersaturation; this is particularly true for proteins, many of which are known to have a high capacity for binding calcium and phosphate. It also possible for adsorbates to block or reduce the efficacy of step sources; this has the effect of reducing the step density and thereby the facet growth rate. In general when impurities are added to the system, the step velocities will change in characteristically different ways (some of which are shown in Figure 9.7) and different mechanisms can be distinguished by measuring the step velocity as a function of adsorbate concentration and mineral supersaturation. In addition to kinetics, AFM images also provide detailed information about which steps are affected by the adsorbate and whether new facets or step morphologies are formed.

We will close with two examples that illustrate different mechanisms of inhibiting crystal growth. The first example looks at a classic step pinning process as peptides interact with a calcium carbonate (calcite) crystal first slowing and finally stopping step propagation. The second example examines the interaction of citrate with DCPD and shows that step kinetics are unaltered but that step density is reduced. In both cases bulk measurements of the crystal growth rate would show inhibition but would not be able to unambiguously pinpoint the mechanism by which this occurred.

9.6.1 Inhibition through step pinning

The classic description of pinning mechanisms is based on impurity adsorption at surfaces, steps or kinks[51-54]. In this case, impurities act as blockers at the sites where they adsorb, preventing the crystal step from propagating locally and thus causing a straight step to become scalloped. As steps curve, their velocity is reduced until they are eventually stopped when their radius of curvature reaches the critical radius (as defined in Section 9.5). In this model, the degree of inhibition depends on the supersaturation and the "blocker" concentration ([X]) on the surface (shown schematically in Figure 9.7b). Higher concentrations of adsorbate cause a greater reduction in velocity and this effects is more pronounced at lower supersaturations. Figure 9.8 illustrates a surface (calcite) where the normally straight steps are being pinned due to adsorbed peptides. At this particular supersaturation and impurity concentration, the steps continue to propagate but are slowed compared to a clean solution at the same supersaturation. A higher resolution image (Figure 8c) shows the tortuous path of the step edge, one of the classic signatures of step-pinning.

9.6.2 Inhibition by reduction of step density

The interaction of citrate with brushite presents a non-intuitive example of how modifiers can be used to tune growth rate. Brushite or apatitic phosphates are often found at the center of kidney stones. It has been suggested that brushite may aid the nucleation of calcium oxalate, the majority component of many stones, and could play a role in the aggregation of crystals to form a stone. Citrate is a common therapy administered to recurrent stone formers and is thought to inhibit crystal growth. In fact, constant composition experiments[40] have shown that citrate does inhibit the growth of

brushite[55]. To investigate the mechanisms by which this occurs, AFM was used to directly image the atomic step kinetics and morphology.

Because citrate forms complexes with calcium in solution, there are two ways of performing this experiment, as shown schematically in a supersaturation versus citrate concentration graph (Figure 9.9a). Citrate can either be added directly to a supersaturated calcium phosphate solution (Expt. 1) or citrate can be added while supplementing calcium to compensate for Ca-citrate complexes that form thus keeping the supersaturaton constant (Expt. 2). While biological realism is always difficult to argue in *in vitro* experiments of this type, expt. 1 may seem a more natural experiment, (after all when you ingest citrate you don't compensate calcium). However, from a crystal growth point of view the experiment designated by expt. 1 has two simultaneous affects: the change in supersaturation and the effects of citrate, which makes interpretation more difficult.

The step velocity data obtained from AFM experiments bear this out. If one uses a titration method (expt. 1) without compensating for complexation, then as one might expect the step velocities decrease when citrate is added (Figure 9.9b, grey diamonds). However by adjusting the calcium to assure a constant supersaturation this effect is removed and the step velocities are constant up to 1mM citrate (Figure 9.9b, black circles).

But in the case where supersaturation is held constant, if citrate does not reduce step velocities and yet does reduce the bulk growth rate, we are left with a puzzle. One possibility is that the step kinetics on facets other than the [010] face are modified. Another possibility presents itself from the AFM images (Figure 9.9); although step velocities and morphology remains unchanged, the *step density* decreases when citrate is added. Because facet growth rate is proportional to both the number and the speed of the steps, a lower density has a concomitant lower facet growth rate.

In spiral growth, the distance between parallel steps (or step density) is a function of the time it takes for new step to begin to propagate As discussed in Section 9.5, this can either be related to the critical length or to the probability of nucleating a kink depending on whether thermodynamics or kinetics dominate. If the steps are in equilibrium, then the decrease in step density implies an increase in the critical length and a concomitant increase in step free energy. On the other hand, if the step motion is kinetically limited the effect of citrate is to decrease the probability of nucleating kinks, which are necessary for step motion. In either case, the interaction with citrate has interesting implications for how organisms might use small amounts of additives to tune crystal growth rate.

This example demonstrates two points. The first is well appreciated, but worth repeating, namely that additives that complex with other ions in the solution can be misidentified as inhibitors if changes in saturation state are not taken properly into account. Second, that bulk crystal growth rates depend not only on the velocity of atomic steps but also on the density of steps. In this example, AFM images showed that citrate molecules inhibit

crystallization not by changing the speed of the atomic steps (as is generally assumed from bulk rate experiments) but rather by modifying the rate at which steps are generated.

9.7 Outlook

Over the past decade, a greater degree of quantification has been made possible through the use of scanning probe microscopy and advanced diffraction techniques. This coupled with a greater control of mineral interfaces through advances in synthesis and genetic engineering and the creation of templates with greater specificity and finer-scaled features, has led to our ability to measure and control biomineral growth to with unprecedented precision.

While it is clear that the understanding and exploitation of self-assembling processes has made great advances, it is equally clear that this is an area of great depth that still has untapped potential. Most bio-inspired assembly processing occurs in aqueous environments, whereas most of the highest-resolution characterization tools are only viable in vacuum. Thus, new experimental tools enabling molecular-level characterization and the monitoring of dynamical processes in fluids would have a great impact on the field as a whole. Future advances will rely on yet faster and higher resolution imaging tools and there is a gaping need for sensitive spectroscopies capable of determining the bonding of surface species. Theoretical advance in crystal growth will need to embrace the complexity of multiple-component crystals and to examine the regime where the generation of kinks is rate-limiting. Overall advances will continue to rely on fundamental understanding of the physical controls on materials assembly from intermolecular force, to activation barriers, to thermodynamics.

Acknowledgement

This work was performed under the auspices of the U.S. Department of Energy by the University of California, Lawrence Livermore National Laboratory under Contract No. W-7405-Eng-48. Portions of this work were supported by the National Institutes of Health (NIDCR grant number DE03223).

References:

[1] R. Z. Wang, L. Addadi, S. Weiner, *Philos T Roy Soc B* **1997**, *352*, 469.
[2] J. F. V. Vincent, *Structural Biomaterials*, Princeton University Press, **1990**.
[3] L. N. Y. Wu, B. R. Genge, D. G. Dunkelberger, R. Z. LeGeros, B. Concannon, R. E. Wuthier, *J Biol Chem* **1997**, *272*, 4404.
[4] N. H. de Leeuw, *Phys Chem Chem Phys* **2004**, *6*, 1860.
[5] S. Mann, J. Webb, R. J. P. Williams, VCH, Weinheim ; New York **1989**, p. 541.
[6] H. A. Lowenstam, S. Weiner, *On biomineralization*, Oxford University Press, New York, **1989**.
[7] E. Bauerlein, *Biomineralization: Progress in Biology, Molecular Biology and Application*, Wiley-VCH, Weinheim, **2000**.
[8] S. Mann, *Principles and Concepts in Bioinorganic Materials Chemistry.*, Oxford University Press, Oxford, **2001**.
[9] R. Z. Legeros, *Calcium Phosphate in Oral Biology and Medicine, Vol. 15*, Karger, Basel, **1991**.
[10] Z. Amjad, Kluwer Academic Publishers, Boston, **1998**, p. 515.
[11] T. Aoba, *Oral Dis* **2004**, *10*, 249.
[12] S. Weiner, W. Traub, *Febs Lett* **1986**, *206*, 262.
[13] G. Daculsi, J. M. Bouler, R. Z. LeGeros, *Int Rev Cytol* **1997**, *172*, 129.
[14] M. Finke, K. D. Jandt, D. M. Parker, *J Colloid Interf Sci* **2000**, *232*, 156.
[15] A. Evan, J. Lingeman, F. L. Coe, E. Worcester, *Kidney Int* **2006**, *69*, 1313.
[16] R. Z. Legeros, *J Dent Res* **1974**, *53*, 45.
[17] J. Abraham, M. Grenon, H. J. Sanchez, C. Perez, R. Barrea, *J Biomed Mater Res A* **2005**, *75A*, 623.
[18] T. Sakae, H. Yamamoto, G. Hirai, *J Dent Res* **1981**, *60*, 842.
[19] G. Faure, P. Netter, B. Malaman, J. Steinmetz, *Lancet* **1977**, *2*, 142.
[20] Z. F. Chen, B. W. Darvell, V. W. H. Leung, *Arch Oral Biol* **2004**, *49*, 359.
[21] R. P. Shellis, *Arch. Oral Biol.* **1978**, *23*, 485.
[22] M. J. Larsen, E. I. F. Pearce, *Arch Oral Biol* **2003**, *48*, 317.
[23] T. Aoba, E. C. Moreno, in *Tooth Enamel IV* (Ed.: R. Fearnheard), Florence, pp. 163.
[24] H. C. Margolis, E. C. Moreno, *Crit. Rev. Oral Bio.* **1994**, *5*, 1.
[25] D. White, State University of New York Buffalo (Buffalo), **1982**.
[26] C. M. Bethke, *Geochemical Reaction Modeling*, Oxford University Press, Oxford, **1996**.
[27] C. Bethke, 5.0 ed., RockWare Inc., Golden, CO.
[28] K. S. Pitzer, *J. Phys. Chem.* **1973**, *77*, 268.
[29] I. S. Harding, N. Rashid, K. A. Hing, *Biomaterials* **2005**, *26*, 6818.
[30] A. A. Chernov, *J Cryst Growth* **2004**, *264*, 499.
[31] H. C. Anderson, *Clin Orthop Relat R* **1995**, 266.
[32] H. C. Anderson, R. Garimella, S. E. Tague, *Front Biosci* **2005**, *10*, 822.
[33] M. Balcerzak, E. Hamade, L. Zhang, S. Pikula, G. Azzar, J. Radisson, J. Bandorowicz-Pikula, R. Buchet, *Acta Biochim Pol* **2003**, *50*, 1019.

[34] L. Zhang, M. Balcerzak, J. Radisson, C. Thouverey, S. Pikula, G. Azzar, R. Buchet, *J Biol Chem* **2005**, *280*, 37289.
[35] R. Robison, *Biochem.* **1923**, *17*, 286.
[36] H. C. Blair, *Bioessays* **1998**, *20*, 837.
[37] A. V. Rousselle, D. Heymann, *Bone* **2002**, *30*, 533.
[38] S. L. Teitelbaum, *Science* **2000**, *289*, 1504.
[39] I. A. Silver, R. J. Murrills, D. J. Etherington, *Exp Cell Res* **1988**, *175*, 266.
[40] G. H. Nancollas, M. B. Tomson, *J Dent Res* **1978**, *57*, 87.
[41] A. Ebrahimpour, J. W. Zhang, G. H. Nancollas, *J Cryst Growth* **1991**, *113*, 83.
[42] P. G. Vekilov, *Prog Cryst Growth Ch* **2002**, *45*, 175.
[43] J. J. De Yoreo, C. A. Orme, T. Land, in *Advances in Crystal Growth Research* (Eds.: K. Sato, Y. Furukawa, K. Nakajima), Elsevier Science, Amsterdam, **2001**, p. 419.
[44] J. J. De Yoreo, P. G. Vekilov, in *Biomineralization, Vol. 54* (Eds.: P. M. Dove, J. J. De Yoreo, S. Weiner), The Mineralogical Society of America, Washington, **2003**, pp. 57.
[45] I. V. Markov, *Crystal Growth for Beginners*, 2nd ed., World Scientific Publishing, Singapore, **2003**.
[46] H. H. Teng, P. M. Dove, C. A. Orme, J. J. DeYoreo, *Science* **1998**, *282*, 724.
[47] A. A. Chernov, L. N. Rashkovich, I. V. Yaminski, N. V. Gvozdev, *J Phys-Condens Mat* **1999**, *11*, 9969.
[48] A. A. Chernov, J. J. De Yoreo, L. N. Rashkovich, P. G. Vekilov, **2004**, *29*, 927.
[49] K. J. Davis, P. M. Dove, J. J. De Yoreo, *Science* **2000**, *290*, 1134.
[50] C. A. Orme, A. Noy, A. Wierzbicki, M. T. McBride, M. Grantham, H. H. Teng, P. M. Dove, J. J. DeYoreo, *Nature* **2001**, *411*, 775.
[51] N. Cabrera, D. A. Vermilyea, in *Growth and perfection in crystals* (Eds.: R. H. Doremus, B. W. Roperts, Turnbull), Wiley, New York, **1958**, pp. 393.
[52] N. Kubota, M. Yokota, J. W. Mullin, *J Cryst Growth* **2000**, *212*, 480.
[53] G. W. Sears, *J. Chem. Phys.* **1958**, *29*, 1045.
[54] K. Sangwal, *Cryst Res Technol* **2005**, *40*, 635.
[55] R. K. Tang, M. Darragh, C. A. Orme, X. Y. Guan, J. R. Hoyer, G. H. Nancollas, *Angew Chem Int Edit* **2005**, *44*, 3698.

Figure Captions:

Figure 9. 1 Schematic graph of supersaturation normalized per growth unit (as defined in equation 9.2) versus the ratio of the activities of calcium and total inorganic phosphate. For $\sigma<0$, solutions are undersaturated and the mineral will dissolve, for $\sigma=0$, the solution is in equilibrium with a solid mineral phase and for $\sigma>0$, the solution is supersaturated with respect to the mineral phase. The slope of the line bounding the metastable region from unstable precipitation can have either a positive or negative slope depending on the kinetics associated with calcium versus phosphate incorporation.

Figure 9.2 A solution map that plots the supersaturation (as defined in equation 9.2) versus a) the ratio of activities of Ca^{2+} and total inorganic phosphate (P_i) and b) the pH for various biological fluids. For each fluid: serum (red), saliva (dark blue), plaque fluid (light blue), enamel (black), and urine (yellow), the supersaturation normalized per growth unit is shown with respect to HAP and DCPD in solid and dotted lines, respectively. The boundaries are approximate based on the range of fluid compositions cited in Table 9.3 and solubility products cited in Table 9.1.

Figure 9.3 Plot of supersaturation (Equation 9.2) versus pH for a range of apatites from the least soluble FAP to the most soluble dentine. The apatites are modeled with the stoichiometry of HAP but with solubility product as cited in Table 9.2. This is not strictly correct but a reasonable approximation for determining a range.

Figure 9.4 Flow setup for in situ AFM experiments. The crystal is imaged while solution flow over the surface.

Figure 9.5 (a,b) Two sequential images showing a growing hillock on the [010] facet of a DCPD crystal. Each image is 2μmx1.5μm and took 12 seconds to capture. Lines and a dot mark the same step in the two images. The step marked with a black line has a lower velocity than the other two steps and does not travel as far. The ratio of terrace widths is proportional to the ratio of step velocities. (c) Atomic model of step geometry with Ca in red, P in blue and O in yellow. The directions on the model are given for space group Ia.

Figure 9.6 Three sequential images showing the growth of etch pits. Pits are labeled P1, P2, and P3.

Figure 9.7 Schematic illustration of how different mechanisms of impurity interactions change the step velocity. As the impurity concentration ([X]) is increased the velocity versus supersaturation (a,b) or velocity versus orientation (c) change in characteristically different t ways. a) Strain caused by the substitution of impurity ions changes the equilibrium solubility (σ_0), which is the concentration where the step velocity goes to zero. This causes the velocity curves to shift over but not change shape. b) Impurities that adsorb to steps can prevent the steps from moving due to the high local curvature of the step between the blocked points. This causes a "dead zone" where the velocity of the steps is slow compared to the clean solution (solid line) c) Surfactants change the step free energy. 2D slices of pseudo Wulff plots of calcite before and after the addition of

aspartic acid, show that the step-edge free energy, $\gamma(\theta)$, changes due to adsorbed molecules at the steps.

Figure 9.8 AFM images of the [104] face of calcite. The crystal is growing in solutions with and without peptide additions. Image (a) is in pure solutions whereas image (b) and (c) are in solution with 6μM of peptide. The steps become pinned (b) when the peptide is added, reducing the velocity of the growth steps. The image in (c) shows the detail of the torturous path of the step edge.

Figure 9.9 Brushite-citrate experiments designed to study the influence of additives on crystal growth. (a) Schematic showing the addition of a complexing agent (in this case citrate) when added to a growth solution (in this case with respect to brushite). Expt. 1 (dotted grey) demonstrates the case when the complexing of citrate with solution calcium is not accounted for resulting in a decrease in the supersaturation of brushite. Expt. 2 (solid black) shows that a constant supersaturation can be maintained by compensating calcium to determine the affect of citrate independently. (b) Actual step velocity data showing a decrease in step velocity when the supersaturation is allowed to vary (grey) but constant when the supersaturation is held constant (black). d-e) AFM images of the same 3μm x 1.5μm area on the [010] face of Brushite The crystal is growing in 37ºC solutions with σ_{gu}=0.14 before (d) and after (e) $2x10^{-6}$ M citrate citrate additions. The density of steps decreases when citrate is added, reducing the growth rate of this facet.

Tables:

Table 9.1 Calcium phosphate minerals and biominerals

Calcium Phosphate	Mineral Name	Chemical Formula	-Log K_{sp} (37°C)	Ca/P[a]
Dicalcium Phosphate (DCPA)	Monetite	$CaHPO_4$	7.04	1
Dicalcium Phosphate Dihydrate (DCPD)	Brushite	$CaHPO_4 \cdot 2H_2O$	6.63	1
β-Tricalcium Phosphate (TCP)	Whitlockite	$Ca_3(PO_4)_2$	29.55	1.5
Octacalcium Phosphate (OCP)	Apatite	$Ca_8H_2(PO_4)_6 \cdot 5H_2O$	97.4	1.33
Hydroxyapatite (HAP)		$Ca_{10}(OH)_2(PO_4)_6$	117.3	1.67
Fluoroapaptite (FAP)		$Ca_{10}F_2(PO_4)_6$	115.8 – 120.2	1.67
Carbonated Apatite (CAP)		$Ca_{10}(OH)_2(PO_4,CO_3)_6$	111.5 – 115.6	
Human Bone[9]		$(Ca,Z)_{10}(PO_4,Y)_6(OH,X)_2$[b]		1.7
Human Enamel[11]		$(Ca,Z)_{9.4}(PO_4,Y)_{5.98}(OH,X)_{1.3}$[b,c]	96.1 – 117.5	1.65
Human Dentine[11]		$(Ca,Z)_{8.96}(PO_4,Y)_{5.96}(OH,X)_{0.78}$[b,d]	88.8 - 104.0	1.61

[a] Molar ratio
[b] Z=Na, Mg, K, Sr, etc; Y=CO_3, HPO_4; X=Cl, F
[c] $(Ca)_{9.12}(Mg)_{0.06}(Na)_{0.22}(HPO_4)_{0.20}(CO_3)_{0.46}(PO_4)_{5.32}(OH,F)_{1.3}$
[d] $(Ca)_{8.44}(Mg)_{0.28}(Na)_{0.24}(HPO_4)_{0.26}(CO_3)_{0.72}(PO_4)_{4.98}(OH,F)_{0.78}$

Table 9.2 Pathological and Normal Calcium Phosphate Minerals found in the body

Tissue	Mineral	Disease	Model solution	Reference
Loops of henle	Apatite, DCPD	Kidney stone formation	Urine	[15]
Teeth	HAP, DCPD, TCP, OCP	Calculus/Caries	Plaque/Saliva	[16, 17]
Salivary glands	DCPD	Sialolith	Saliva	[18]
Joint	DCPD, HAP	Rheumatoid & osteoarthritis	Synovial (joint) fluid	[19]

Table 9.3 Composition ranges (in mM) of human fluids and associated mineral saturation states of phosphates.

	Serum	Saliva[21, 22]	Enamel Fluid[23]	Plaque Fluid[24]	Urine[25]
Na^+	130 - 150	10	140	6.8 - 50	50 - 250
Cl^-	99 - 110	23	150	14 - 52	64 - 380
Ca^{2+}	2.1 - 2.9	0.40 - 2.1	0.5	0.8 - 8.6	0.81 - 7.8
P_i	0.74 - 1.5	2.9 - 11	3.9	7.8 - 29	7.2 - 45
HCO_3^-	8.2 - 9.3	2.1 - 25	10		
K^+	3.6 - 5.6	23	21	38 - 90	20 - 96
Mg^{2+}	0.74 - 1.5	0.21	0.8	1.3 - 5.5	0.70 - 7.8
F^-	0.01 - 0.02	0.005	0.005	0.0013 - 0.018	
SO_4^{2-}	0.08 - 0.12				0.50 - 50
NH_4^+		4		19 - 64	10 - 56
Growth Parameters					
pH	7.4	5.5 - 7.5	7.2 - 7.3	5.69 - 7.08	4.8 - 8.0
{Ca}/{P_i}	1.31 - 2.54	0.02 - 0.69	0.145[a]	0.01 - 1.40	0.05 - 1.89
I (mM)	152 - 153	39 - 46	165 [a]	152 - 155	258 - 274
σ_{gu} DCPD	-0.9 - -0.5	-1.6 - 1.0	-0.50 [a]	-1.1 - 1.7	-2.1 - 1.6
σ_{gu} TCP	0.8 - 1.2	-1.6 - 2.6	0.81 [a]	-1.2 - 3.0	-2.7 - 3.5
σ_{gu} OCP	0.4 - 0.8	-1.3 - 2.0	0.49 [a]	-0.9 - 2.4	-2.1 - 2.7
σ_{gu} HAP	2.3 - 2.7	-0.2 - 3.8	2.22 [a]	0.2 - 4.2	-1.3 - 4.8

[a] Average values

Table 9.4 Crystal growth controls and their effect on the bulk solution and the crystal surface.

Parameter (symbol)	Effect on Bulk Solution	Effect on Surface
Supersaturation (S)	Stability of solid phases	Net flux to surface; Determines mode of growth (island nucleation versus incorporation at existing steps).
pH	Solution speciation (and subsequently supersaturation)	Net charge of surface due to degree of protonation
Ionic Strength (I)	Screening length within the solution – activity coefficients	Debye Length of the double layer
Temperature (T)	Solution speciation through temperature dependence of association constants	Kinetics of adsorption, desorption, diffusion
Ratio of calcium to phosphate ions $\{Ca^{2+}\}/\{P_i\}$	Solution speciation	Kinetics of incorporation – in principle, activation barriers differ for calcium and phosphate ions
Additive concentration ([X])	Can change solution speciation (and subsequently supersaturation)	Various: Step-pinning, Surfactant, Blocking layer, Incorporation, etc.

Table 9.5: Examples of biological regulation that change the mineralizing fluid.

Cell Activity	Biological regulation	Potential Effect on Mineralization	Base fluid
Bone growth	Osteoblasts produce enzyme Akaline Phosphatase	Increase P_i	Matrix Vesicle
Bone growth	Osteoblasts produce enzyme Akaline Phosphatase	Reduce inhibitor concentration	Matrix Vesicle
Bone resorption	Osteoclasts activate H+-ATPase pump	Decrease pH	Resorption Lacuna/serum
Tooth dissolution (caries)	Bacteria produce lactic acid	Decrease pH	Saliva or plaque

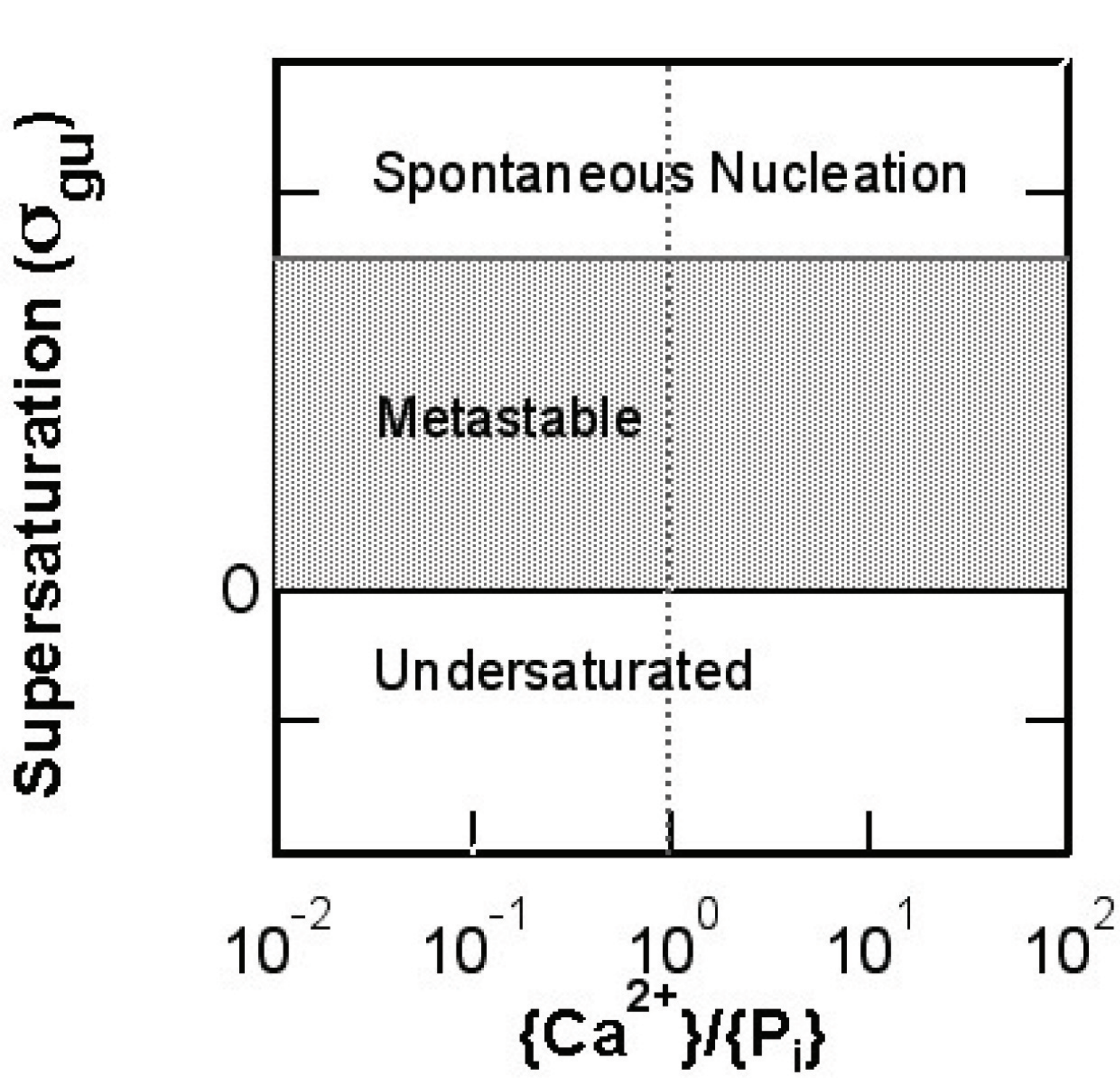
Supersaturation (σ_{gu})
Spontaneous Nucleation
Metastable
0
Undersaturated
10^{-2}
10^{-1}
10^{0}
10^{1}
10^{2}
$\{Ca^{2+}\}/\{P_i\}$

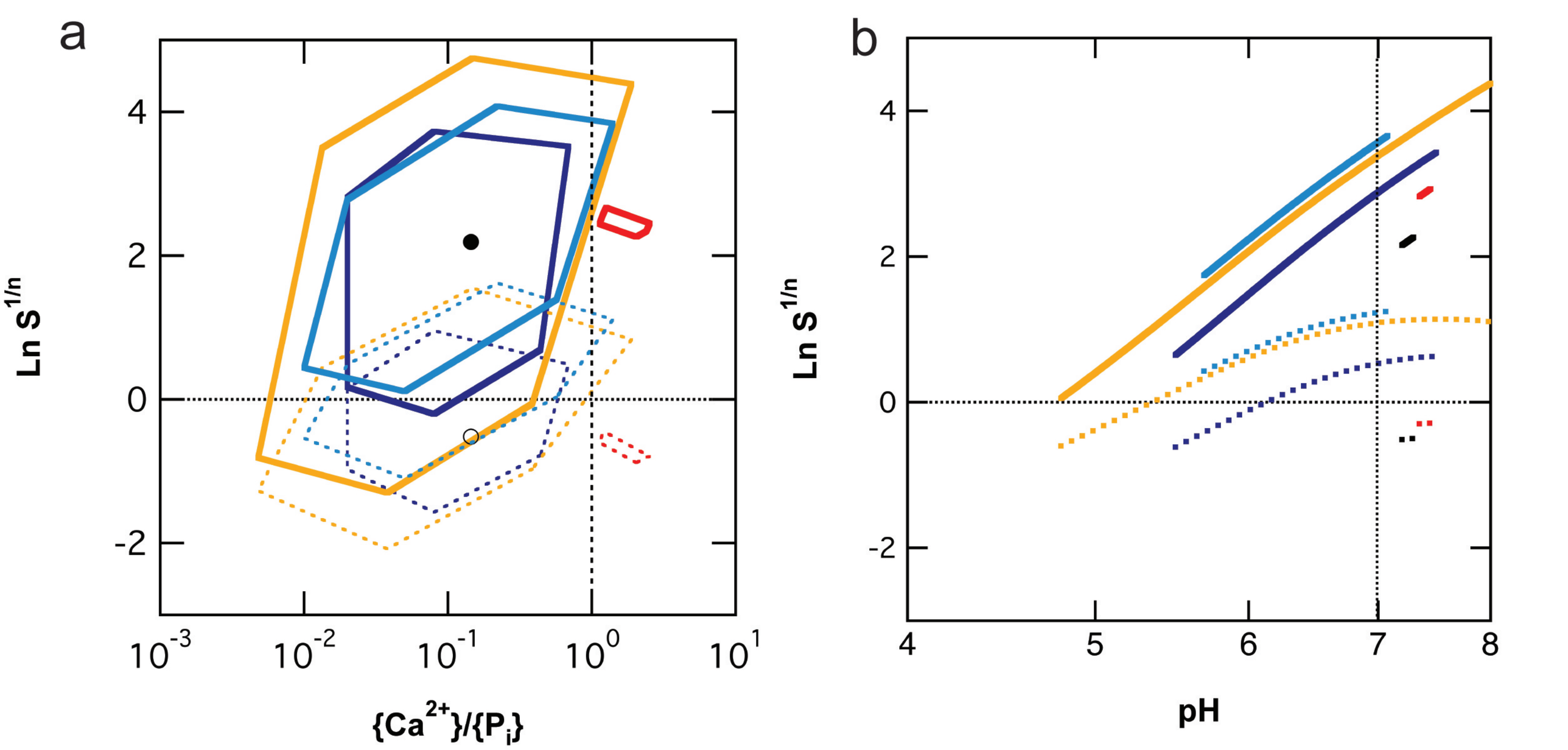
a
b
Ln S^1/n
{Ca2+}/{Pi}
pH
4
2
0
-2
10-3
10-2
10-1
100
101
5
6
7
8

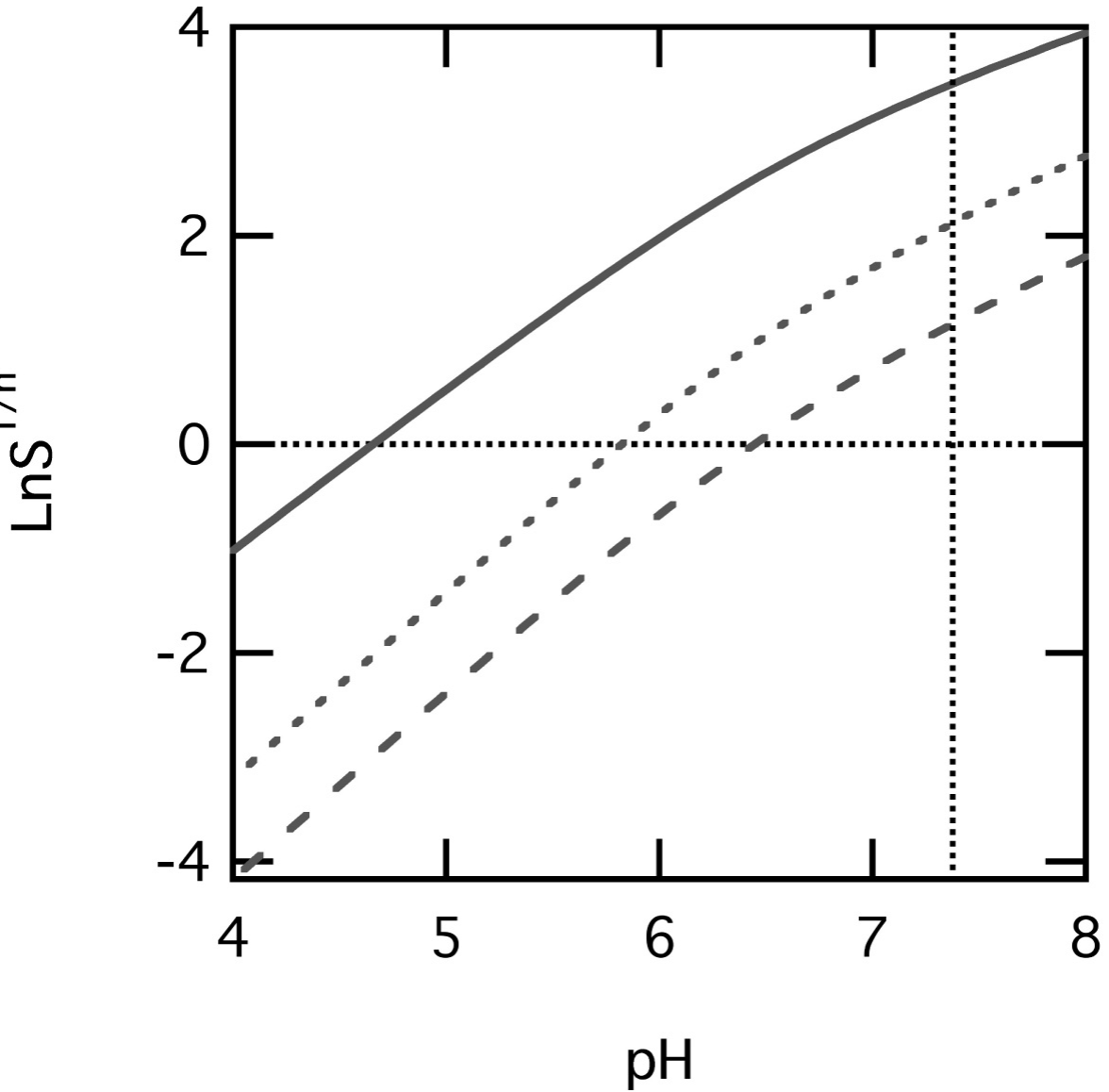
4
2
0
-2
-4
4
5
6
7
8
LnS^1/n
pH

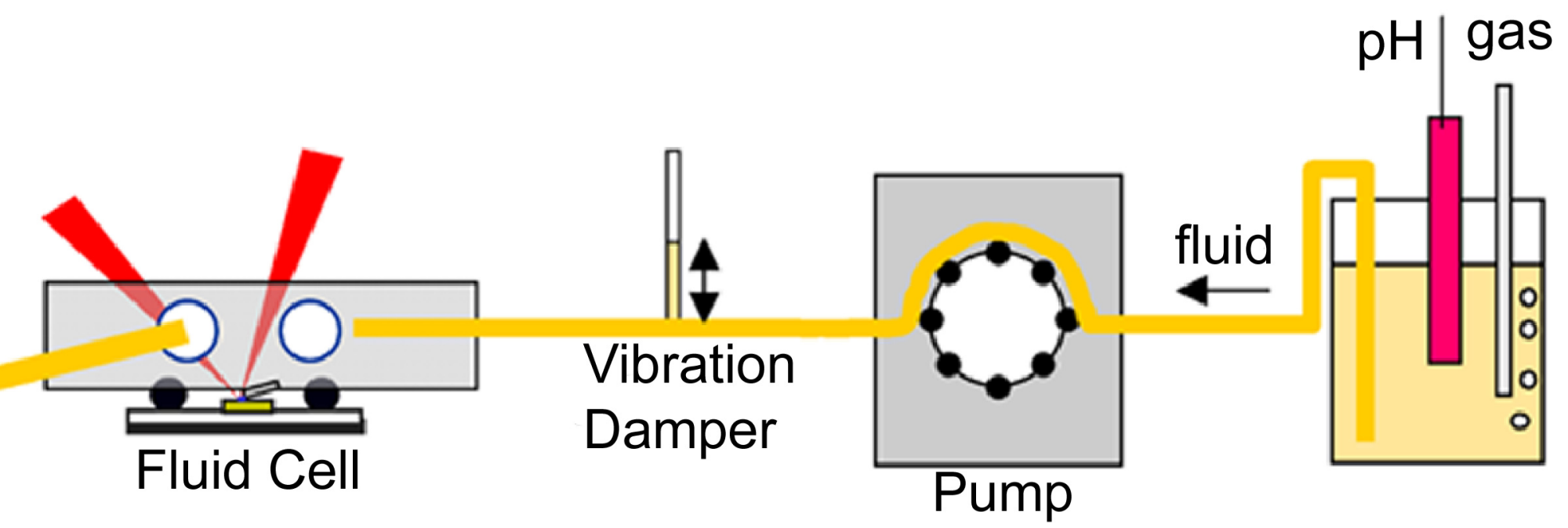
pH
gas
fluid
Vibration
Damper
Fluid Cell
Pump

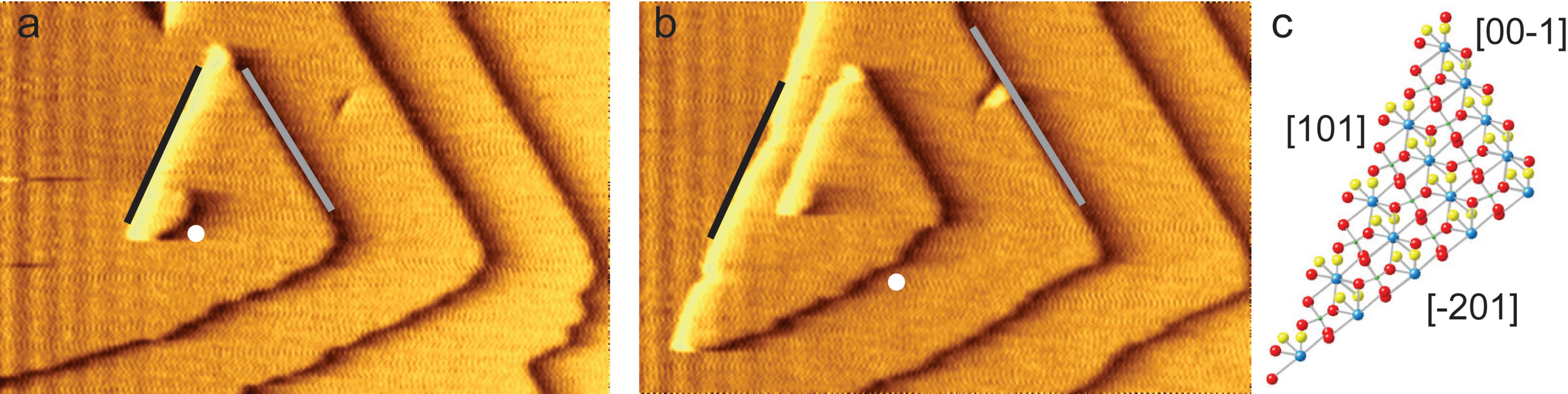
a
b
c
[00-1]
[101]
[-201]

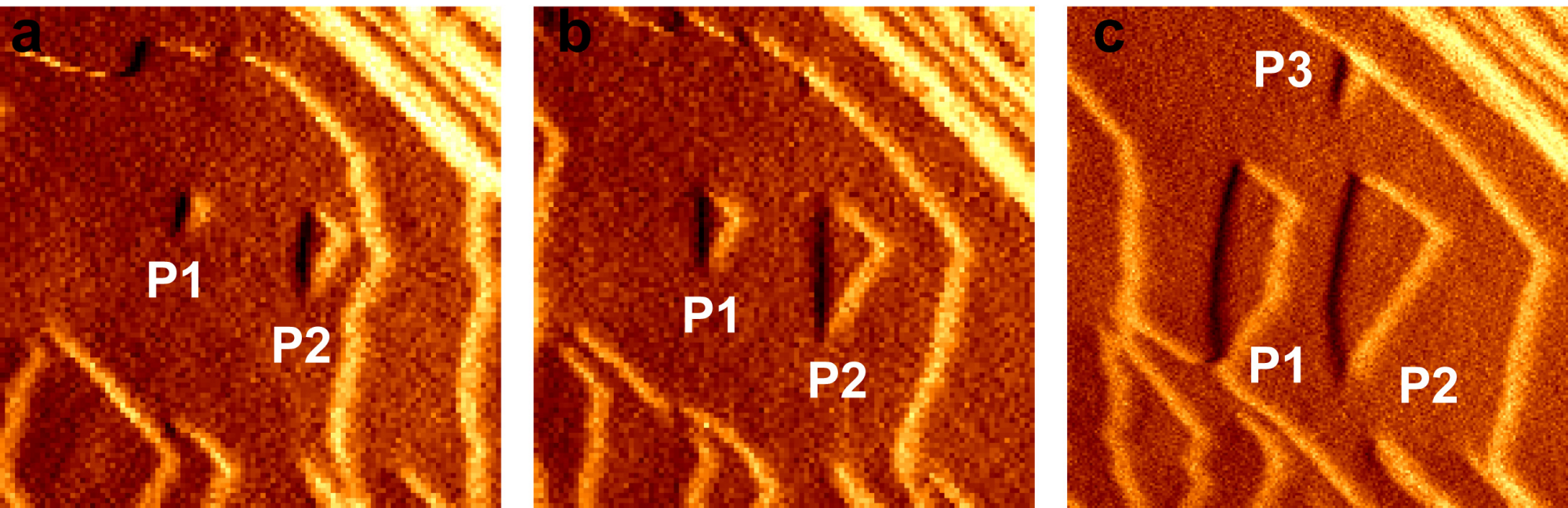
a
P1
P2
b
P1
P2
c
P3
P1
P2

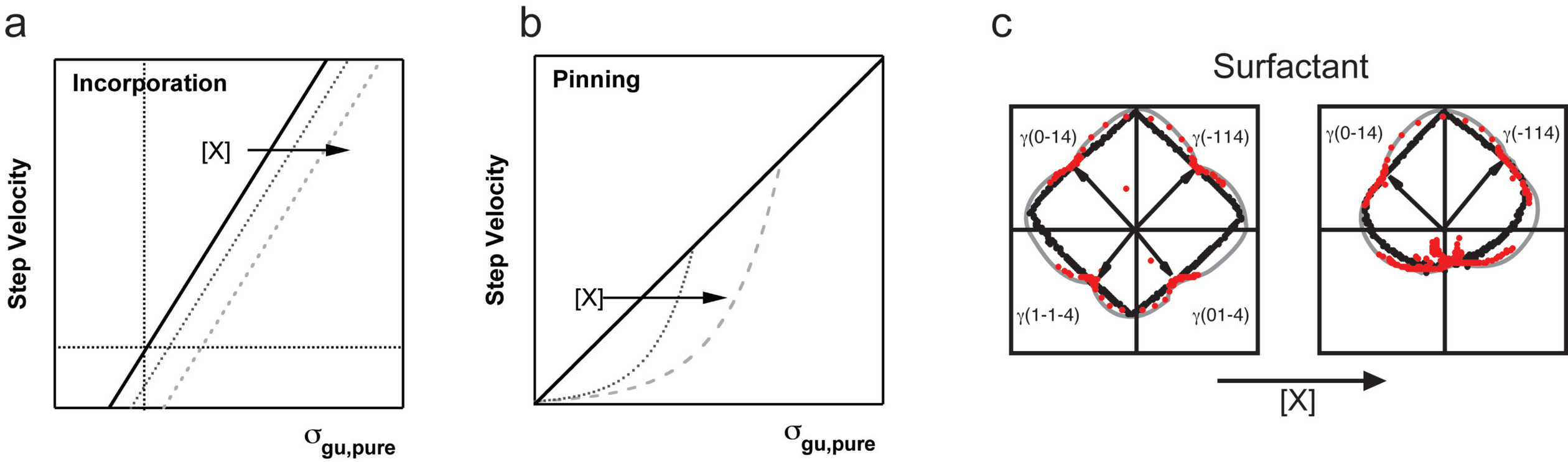
a
Incorporation
[X]
Step Velocity
σgu,pure
b
Pinning
[X]
Step Velocity
σgu,pure
c
Surfactant
γ(0-14)
γ(-114)
γ(1-1-4)
γ(01-4)
γ(0-14)
γ(-114)
[X]

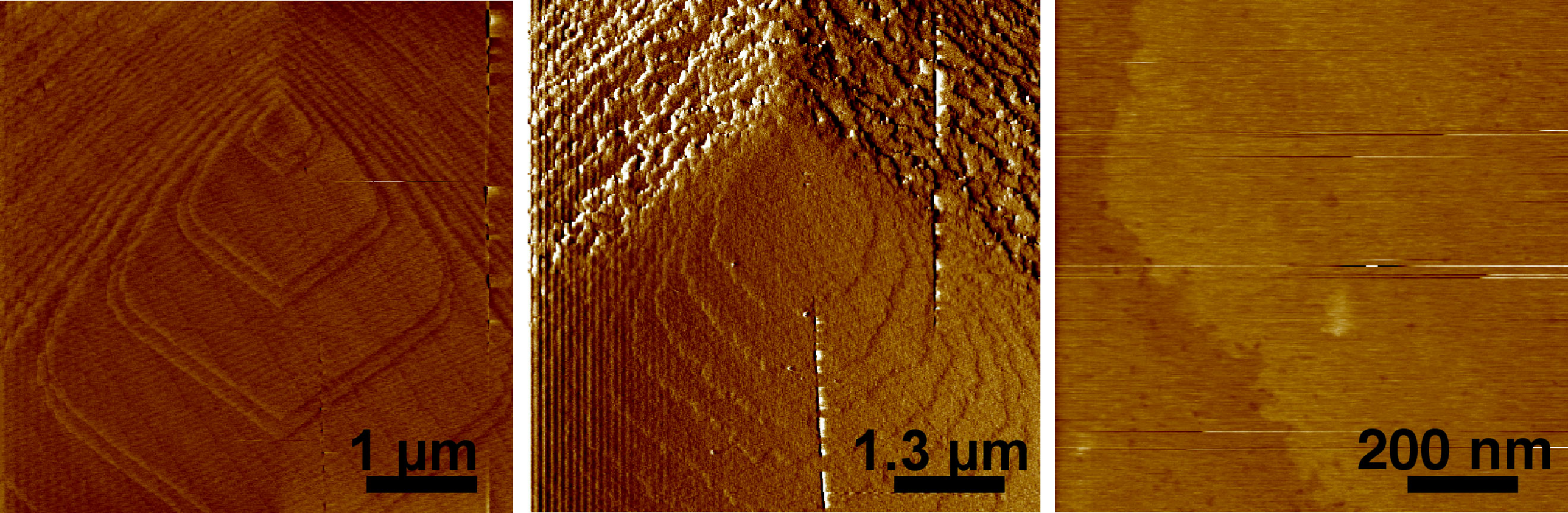
1 µm
1.3 µm
200 nm

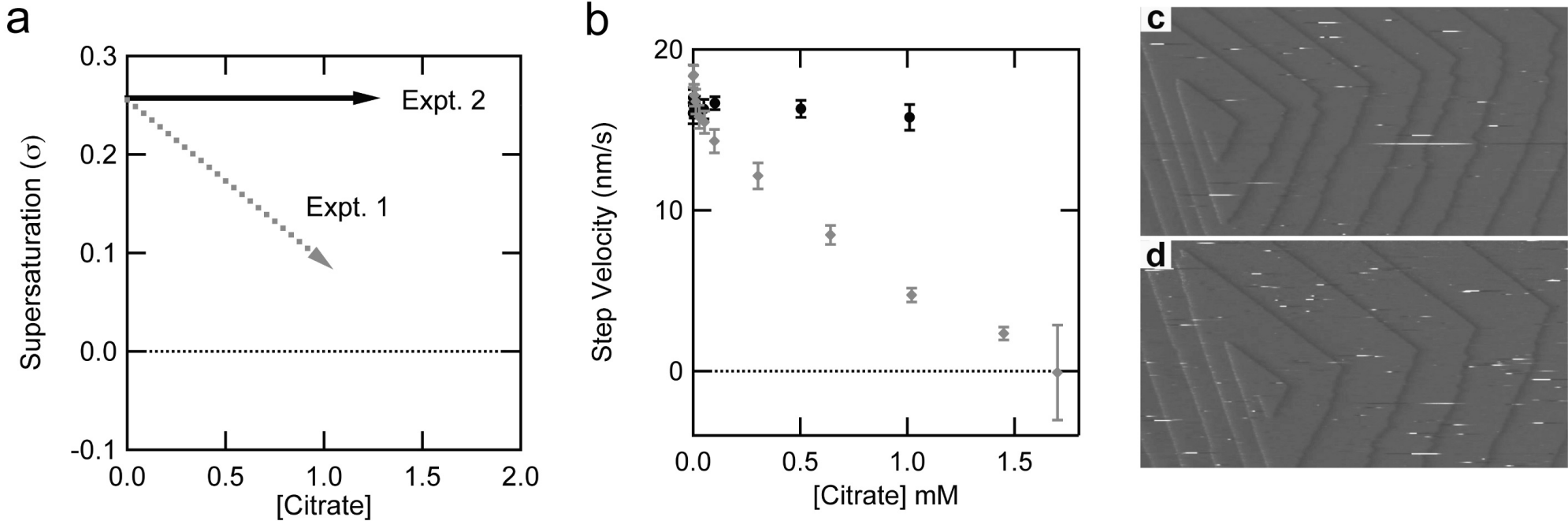
a
0.3
0.2
0.1
0.0
-0.1
Supersaturation (σ)
Expt. 2
Expt. 1
0.0
0.5
1.0
1.5
2.0
[Citrate]
b
20
10
0
Step Velocity (nm/s)
0.0
0.5
1.0
1.5
[Citrate] mM
c
d